



# Effect of Various Welding Parameters on Corrosion Behavior of Friction-Stir-Welded AA 7075-T651 Alloys

Pratik H. Shah<sup>1,2</sup>  · Vishvesh Badheka<sup>3</sup>

Received: 3 November 2017 / Revised: 16 March 2018 / Accepted: 31 March 2018 / Published online: 12 April 2018  
© Springer Science+Business Media, LLC, part of Springer Nature and ASM International 2018

## Abstract

The 7000 series aluminum alloys provide the highest strength of all aluminum alloys and are widely used in the aerospace industries. They are practically unweldable by conventional fusion welding techniques. Friction stir welding is a widely accepted process to join this material. The paper intends to evaluate the electrochemical behavior of friction-stir-welded AA 7075-T651 alloy under varying welding conditions. An attempt has been made to evaluate the effect of tool rotation speed, welding speed, and shoulder diameter on its corrosion characteristics. The temperature histories during welding were continuously recorded with the help of thermocouples. The corrosion characteristics have been examined as per ASTM G-34 standards. The analysis is done by immersing the plates in EXCO solution and analyzing through optical imaging, SEM and TEM. The analysis revealed that the heat-affected zone was found to be most susceptible to corrosion. The corrosion resistance is found in the order—weld nugget > unwelded base metal > HAZ. The experiments revealed that the corrosion resistance of the welded plates is directly proportional to the heat input during the welding process. The plates welded with lower tool rotation speed, higher welding speed, and lower shoulder diameter exhibited higher corrosion resistance.

**Keywords** Friction stir welding · Corrosion · Aluminum 7075-T651 · EXCO · Intermetallics · Pitting

## Introduction

Aluminum alloy 7075 has received special attention in industries today due to its high strength. Certain important qualities such as its high strength-to-weight ratio coupled to its capability to naturally age make it suitable for applications involving various aircraft structure [1]. The major alloying elements contained in this material are

copper, zinc, and magnesium. The precipitates of  $Al_2CuMg$  and  $Mg_2Zn$  phases mainly accounts for the high strength of the material [1, 2]. The precipitation hardenable 7000 series aluminum alloys are being extensively used in the various components of an aircraft structure, military vehicle, earth-moving equipments, bridges, and other highly stressed defense applications [3, 4]. Fusion welding of these alloys is extremely difficult as it is highly sensitive to weld solidification cracking. This limits the use of AA 7075 in major applications that involve fusion welding [5, 6]. Friction stir welding (FSW), a solid-state welding, is a feasible process to join alloys that are difficult to join by convention fusion welding techniques [7]. The Welding Institute (TWI) at Cambridge holds the privilege of inventing friction stir welding (FSW) process. The process is credited for being a green technology, energy efficient, and a solid-state process capable of welding light alloys that are practically unweldable by fusion joining processes [2, 3]. It utilizes a tool with a profiled pin and shoulder having special design features. The tool does not consume during the process. During the process, the pin is forced

---

✉ Pratik H. Shah  
p1shah55@yahoo.com; p1shah55@gmail.com  
Vishvesh Badheka  
vishvesh79@gmail.com

<sup>1</sup> Department of Mechanical Engineering, Faculty of Technology, Charusat University, Changa, Gujarat 388421, India

<sup>2</sup> Sardar Vallabhbhai Patel Institute of Technology (SVIT), Vasad, Gujarat 388306, India

<sup>3</sup> Department of Mechanical Engineering, School of Technology, Pandit Deendayal Petroleum University, Gandhinagar, Gujarat 382007, India

into the plates to be joined at a predetermined rotational speed. The combined effect of the frictional heat produced by the action of the tool shoulder rubbing with the plates and plastic displacement resulting due to the rotating pin creates the joint between the plates in pure solid form [8]. During the process, the tool traverses the weld joint at a constant feed rate. Since the entire process takes place in solid state, many defects associated with conventional fusion welding can be eliminated [9]. The quality of the weld largely depends upon the process variables viz. tool rotational speed, weld traverse speed, and tool design [10]. Friction stir welding seems to be one of the most promising techniques for joining aluminum alloy 7075-T651 avoiding the potential problem of solidification cracking. 7075-T651 aluminum is practically unweldable by fusion processes. The microstructure of a FSW joint is typically characterized by three regions (a) the weld nugget (WN) or the stir zone consisting of fully recrystallized grains resulting due to heat and stirring action of the pin, (b) the thermomechanically affected zone (TMAZ) immediately adjacent to the stir zone of both the sides where the grains are plastically elongated but not recrystallized, and (c) the heat-affected zone (HAZ), where the material experiences no plastic deformation but is influenced by the heat of welding leading to some microstructural changes [10]. Though FSW is a solid-state welding process, the non-uniform temperature distribution results into different precipitate morphologies in these regions [7, 11]. The welding temperatures result into dissolution/coarsening of the precipitates in varying proportions in the weld regions [12–14]. The precipitation dissolution during the process not only affects the joint properties but also affect the electrochemical behavior of the welded alloy [15]. Thus the different weld regions exhibit different corrosion resistance.

Research in the past has proved that though FSW results in reasonably sound welds, the weld joints have been observed to be susceptible to intergranular, pitting, and exfoliation corrosion. This is especially true for friction-stir-welded heat-treatable aluminum alloys like 7xxx and 2xxx series. It was observed by Lumsden et al. [16] that the weld zones of friction-stir-welded AA 7075-T651 were susceptible to intergranular corrosion with the HAZ most vulnerable to intergranular corrosion. Khoshnaw and Gardi [17] observed exfoliation corrosion in both AA 7075-T6 and AA 2024-T3, but found that with increase in the aging time the corrosion resistance of AA 2024-T3 alloy decreased while that of AA 7075-T6 alloy increased. Venugopal et al. [18] observed that the corrosion resistance of the nugget zone was better than that of the base metal and TMAZ. Andreatta et al. [19] observed that the temper of the high-strength aluminum alloys significantly affects their corrosion susceptibility. They observed that the peak aged temper (T6) of AA7075 alloy was more susceptible to

intergranular and pitting corrosion than compared to over-aged temper (T7). Dey et al. also observed the same phenomena wherein they found that the T73 temper of AA 7075 has superior corrosion resistance as compared to the T6 temper but found that there was a marked deprivation in the strength properties of the T73 temper. The intermetallic phases and the phases in the grain boundaries largely influence the corrosion behavior of the friction-stir-welded aluminum alloys. In particular, the friction-stir-welded zones in heat-treatable aluminum alloys are more sensitive to corrosion than compared to the aluminum matrix. The strength and ductility of the friction-stir-welded AA 7075-T6 alloys are dependent on the grain size, the size, and presence of coherent intragranular precipitates, whereas the corrosion behavior is controlled by the intermetallic phases as well as the grain boundary phases and/or precipitate-free zones [20]. The pitting corrosion, which is a very common corrosion phenomenon in friction-stir-welded aluminum alloys, is initiated by intermetallic Al–Cu–Fe–Mn–(Si) phase [21]. The corrosion pits normally form by grooving around these intermetallic particles [22, 23].

AA 7075 sheet and plate products are being used throughout aerospace structures such as fuselage frames/bulkheads, fuselage stringers, fuselage skin, wing upper stringer, wing upper skin, wing lower stringers, and lower wing panels [24]. As discussed, the alloy has a very poor weldability by fusion welding, and hence it is welded by FSW process. It has been reported that friction-stir-welded AA 7075-T651 alloy has been susceptible to corrosion. However, very limited information is presently available on the effect of various process parameters on the corrosion susceptibility of AA 7075-T651 alloy. The investigation aims at studying the effect of various important parameters (viz. tool rotational speed, welding speed and shoulder diameter) on the corrosion characteristics of friction-stir-welded AA 7075-T651 alloy. The study also investigates the effect of weld heat input on the corrosion susceptibility of the alloy.

## Materials and Methods

The base material selected for investigation is AA 7075-T651 alloy. The thickness of the base material is 6.5 mm and is procured under the sponsored project E33011/60/2010-V of Indian Space Research Organisation (ISRO), Ahmedabad. The alloy contains zinc, magnesium, and copper as its major alloying elements. The chemical composition of the base metal is shown in Table 1. The experiments are conducted on a special experimental setup of FSW, procured under the same project. A specially designed fixture made from SS 304 is used to rigidly clamp

**Table 1** Chemical composition of the base material (AA 7075-T651)

Si	Fe	Cu	Mn	Mg	Zn	Cr	Ti	Al
0.025%	0.142%	1.21%	0.032%	2.126%	6.045%	0.128%	0.056%	Balance

**Table 2** Friction stir welding parameters

Process and tool parameters	Units	Notation	Values		
Tool rotation speed	(rpm)	N	765	1070	1500
Welding speed	(mm/min)	S	20	31.5	50
Shoulder diameter	(mm)	D	18	20	22

the plates during the welding process. The fixture also does the function of the backing plate. The use of stainless steel helps in retaining the heat at the rear side of the workpiece, due to its low thermal conductivity. The fixture was mounted on the table of the vertical milling machine, and the plates were clamped on the fixture with zero root gap. The fixture helped in restricting the movement of the plates under the action of plunging and weld traverse forces of the welding tool.

Three parameters each at three levels were used to fabricate six joints. The process and tool parameters are present in Table 2. The experiments were performed using non-consumable tools fabricated from H13 steel. Three tools with different shoulder diameters and cylindrical threaded pin profile were used. Figure 1 shows the dimensions of the tools. The tilt angle (TA) of the tool relative to the plates was kept at 3°.

Special provisions in the workpiece were made in order to measure the temperatures on the advancing and the retreating sides during the welding process. The temperatures on the advancing and retreating sides were recorded with K-type thermocouples having sheath diameter of 1.5 mm. The maximum temperature measuring capacity of the thermocouple is around 1100 °C. In order to record the temperatures, two holes with a diameter of 2 mm and depth of 40 mm at 50 mm traverse length (as shown in Fig. 2) were drilled on the sides of the plates to accommodate the thermocouples. The holes were drilled in the middle in the thickness direction of the workpiece's side edge so that the thermocouples are placed along the transverse direction. It was ensured that the holes made for accommodating the thermocouples were deep enough to properly secure the thermocouples. This ensures that the temperature measurement is correct without any disturbances. The position of the thermocouples is so decided that it measures the temperatures just near to the rim of the tool shoulders. This position also ensures that the probes are not damaged by the stirring action of the tool.

The temperatures were recorded continuously using ENVADA make multi-loop scanner with 16 channels. The scanner was connected to a personal computer that had a

data acquisition system called eScan 9.0 installed to record the temperature histories during the process. The temperatures are recorded at a time interval of 3 s as the welding progressed. Figure 3 shows the setup of the experiment. The average of the peak temperatures recorded on the advancing and the retreating sides is taken into consideration for further investigations. The temperature profiles for various experiments are plotted.

Once the plates and the tool were mounted, the sensing tip of the thermocouples was inserted in the holes to secure the position at the desired locations in the plates. The other end of the thermocouples was connected to the ENVADA scanner and the scanner was connected to a laptop. The laptop has a preinstalled data acquisition software eScan 9.0 which records the temperatures at a preset time intervals. The required tool was fitted into the spindle of the machine. After the setup was ready, the joint line was aligned with the centerline of the FSW tool. The tool rotation speed, traverse (welding) speed, and the tilt angle of the machine table were set prior to each welding run. Then the machine is switched on and the rotating tool is slowly plunged into the workpiece (at the predrilled hole of 4 mm diameter). The tool pin is slowly plunged into the workpiece at a rate of 0.05 mm/min until it is visually ensured that the tool's shoulder contacts the upper plate surface. The tool shoulder was then plunged by 0.1 mm (plunge depth) below the top surface of the plates. After a dwell time of 30 s, the machine bed movement was switched on. The tool is forcibly traversed along the weld line at a preset traverse rate until the tool reaches the end of the weld. On reaching at the end of the weld, the traverse movement of the bed is stopped and the welding tool is retracted from the workpiece while the machine spindle continues to rotate. After the tool is completely retracted from the plates, the machine spindle is stopped. The pin of the tool leaves a hole generally known as the exit hole in the workpiece the end. The welded plates are then unclamped after substantial heat loss from the plates takes place. The temperature recording is stopped, and the thermocouples are retracted from the holes. Six experiments were conducted: two each for studying the effect of tool

**Fig. 1** Dimensions of the tools  
(a) 18 mm, (b) 20 mm and  
(c) 22 mm shoulder

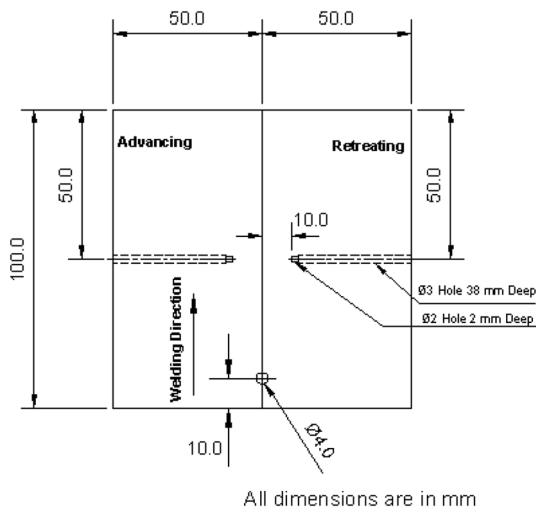
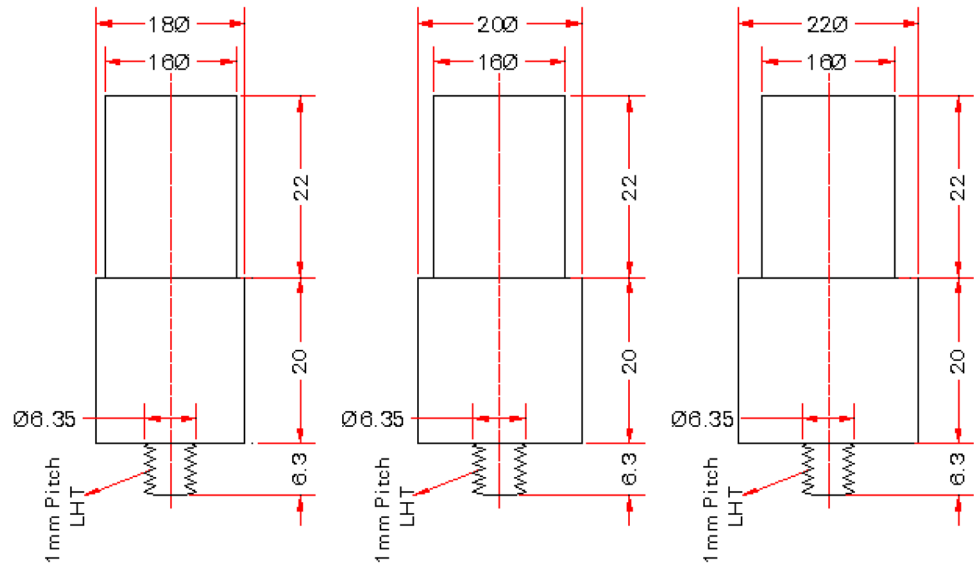


**Fig. 2** Workpiece dimensions and the locations of the thermocouples

rotation speed, welding speed, and shoulder diameter. The process parameter combinations were so selected that they would result in the highest and the lowest weld heat input condition for a particular parameter under study. The parameter combinations for which the experiments were conducted are shown in Table 3.

**The Corrosion Testing Methodology**

The methodology adopted for this study is forced corrosion of the plates by immersion in a highly corrosive medium. The corrosion susceptibility of welded plates is tested as per ASTM G-34 standard by immersing the test specimens in EXCO solution. The EXCO test which is a favored test for the evaluation of corrosion for aerospace alloys provides an accelerated corrosion test for 2xxx and 7xxx series

aluminum alloys. For this test, the welded samples along with a sample of unwelded base plate are immersed in a highly corrosive solution containing 4 M sodium chloride, 0.5 M potassium nitrate, and 0.1 M nitric acid. The specimens were maintained at a temperature of 25 °C for a period of 48 h. The weld region which was the area of interest was exposed to the test solution, while the rest of the portion was masked with styrene–butadiene polymer tape. The analysis of corroded plates is done with the help of optical microscopy, scanning electron microscope (SEM)/energy-dispersive X-ray spectroscopy (EDX) and transmission electron microscope (TEM).

**Results and Discussion**

The detail discussion on the corrosion characteristics of all the specimens follows.

**Unwelded Base Metal**

It is seen that the friction-stir (FS)-welded plates show much higher surface degradation than compared to the unwelded base plate (Ref. Fig. 4). Similar observations have been reported by Venugopal et al. [18]. The photographs of the corroded unwelded and the welded plates show pitting on the surface. The SEM image of the unwelded base metal after immersion in EXCO solution for 48 h is shown in Fig. 5. The image shows intergranular cracks (IGC) with general discoloration over the surface. It also indicates that the corrosion on the surface is a combination of pits and intergranular cracks, with intergranular corrosion being more visible. The localized corrosion initiates as pitting and propagates as intergranular corrosion



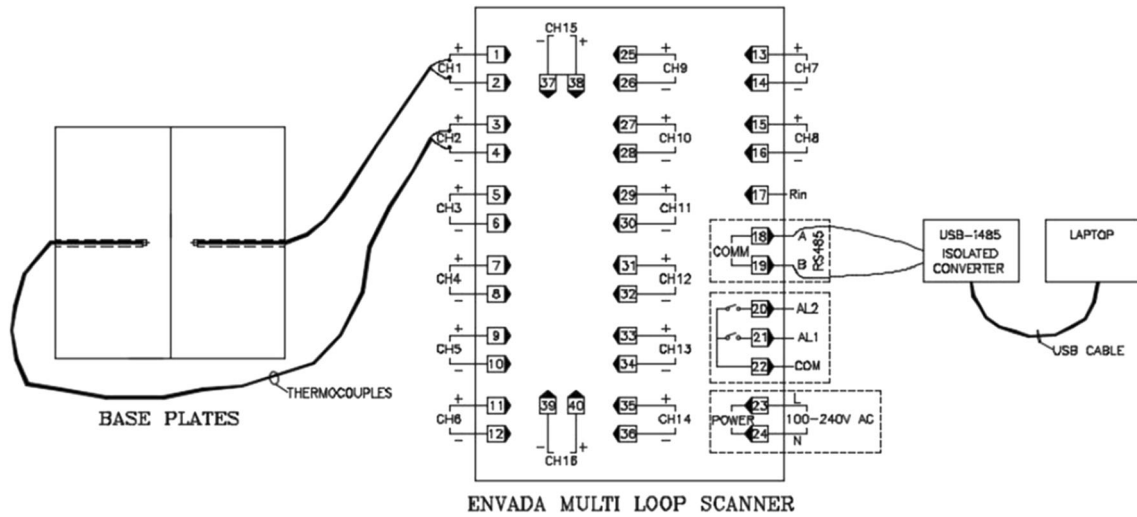


Fig. 3 Welding setup and location of thermocouples

Table 3 Parameters selected for experiments

Sample ID	N, rpm	S, mm/min	D, mm	TA, degrees
For tool rotation speed				
C1	1500	20	22	3
C2	765	20	22	3
For welding speed				
C3	1070	20	20	3
C4	1070	50	20	3
For shoulder diameter				
C5	1500	50	22	3
C6	1500	50	18	3



Fig. 4 Image of Al 7075-T651 unwelded base plate exposed for 48 h in EXCO solution

which is in accordance with findings reported by Paglia et al. [25]. The second-phase particles (intermetallics) found in the matrix are the major cause of the pit formation as the intermetallics are the nucleation sites for the localized corrosion. AA 7075-T651 is a Al–Zn–Mg–Cu series alloy. The particles containing Al, Zn, and Mg are anodic in nature while that containing Al, Fe, Cu, and Mn are cathodic in nature. Both the anodic and cathodic particles demonstrate different electrochemical activity and passivation ability in comparison with the surrounding matrix [26, 27]. The galvanic coupling between the intermetallics and the surrounding matrix results in pit formation. The

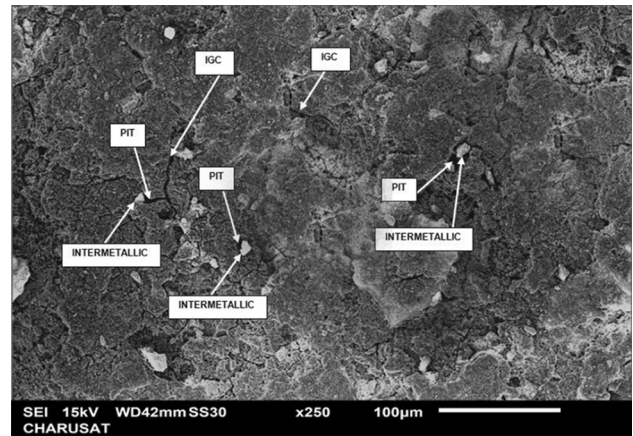


Fig. 5 SEM image of corroded unwelded base metal Al 7075-T651 post-immersion in EXCO solution showing pits and intergranular cracks

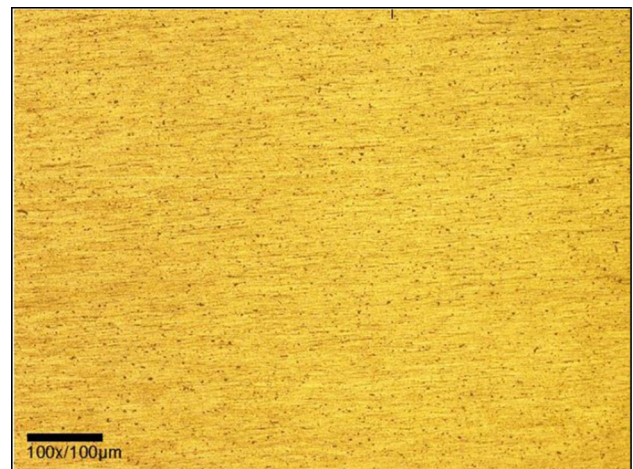
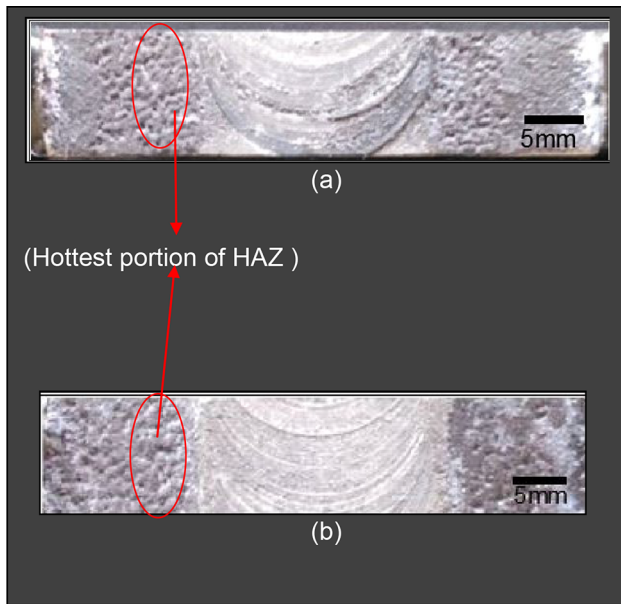
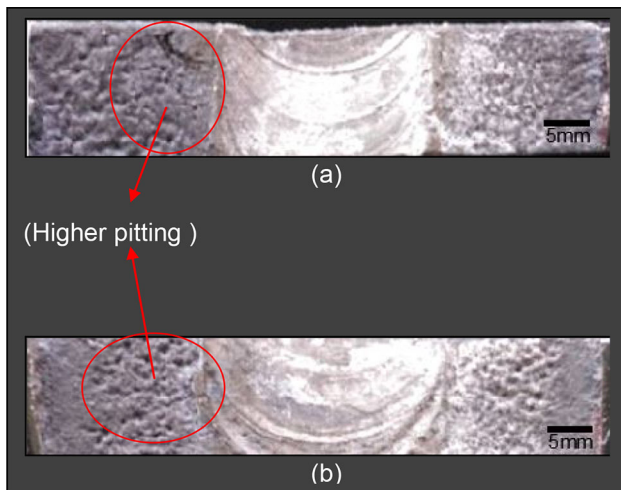


Fig. 6 Optical micrograph of the base material (100x)



**Fig. 7** Image of Al 7075-T651 welded specimens at variable TRS exposed for 48 h in EXCO solution. (a) Sample C1. (b) Sample C2



**Fig. 8** Image of Al 7075-T651 welded specimens at variable WS exposed for 48 h in EXCO solution. (a) Sample C3. (b) Sample C4

intermetallic particles containing Fe and Cu are cathodic to the matrix and results in dissolution of the matrix. The particles containing Zn and Mg are anodic to the matrix and dissolve preferentially [19]. Thus both anodic and cathodic particles can induce pitting corrosion.

The pits have been observed to form around the intermetallics. The SEM/EDX analysis undertaken for FS-welded plates (covered later in this study) has established that the intermetallics consist of Al, Fe, and Cu in different proportions. The intermetallics found in the matrix are cathodic to the aluminum matrix and results in the matrix being attacked resulting in the formation of pits. The

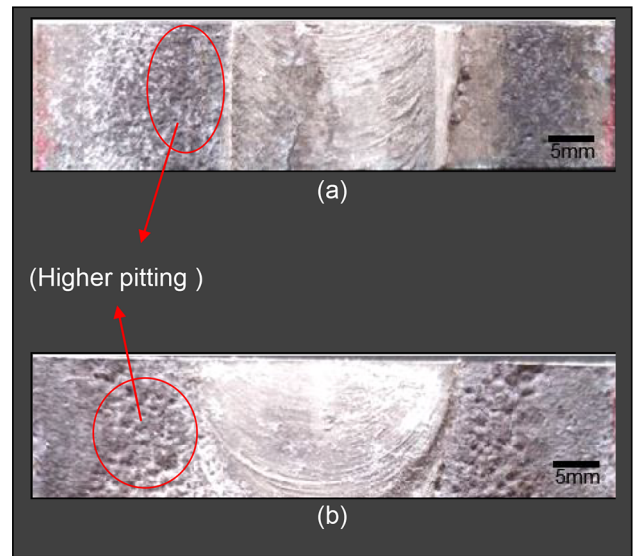


**Fig. 9** Image of Al 7075-T651 welded specimens at variable SD exposed for 48 h in EXCO solution. (a) Sample C5. (b) Sample C6

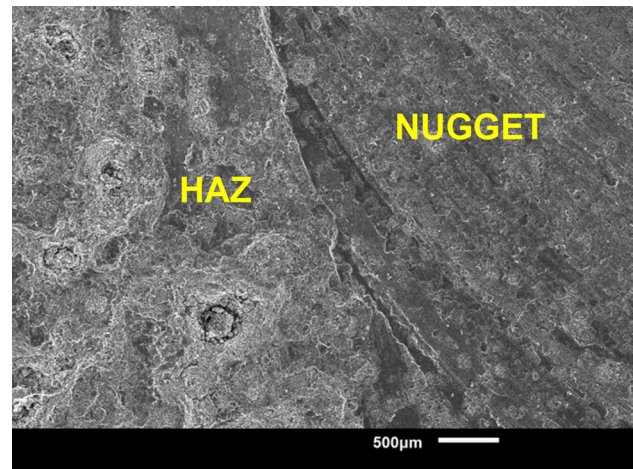


**Fig. 10** Low-magnification SEM image of corroded weld sample showing WN and HAZ

intermetallics initiate pitting at the surrounding matrix and also enhance the pit growth. Hence pits have formed in the aluminum matrix near to the Cu or Fe intermetallics. Figure 6 represents the microstructure of base metal consisting very fine insoluble second-phase precipitates dispersed in various locations of elongated grains.

### Corrosion in the Welded Plates

The surface of the friction-stir-welded plates indicates that the corrosion resistance of the welded plates is much lesser than compared to the unwelded base plates. As indicated earlier, two set of welded plates for each parameter (viz. the tool rotation speed, welding speed, and shoulder diameter) are investigated post-immersion into the EXCO



solution for 48 h. The weld nugget of all the welded plates irrespective of the welding parameters was least affected. The hottest area in the HAZ portion immediately flanking to the tool shoulder was found to be most vulnerable to corrosion (Refer Figs. 7, 8, 9). The SEM image shown in

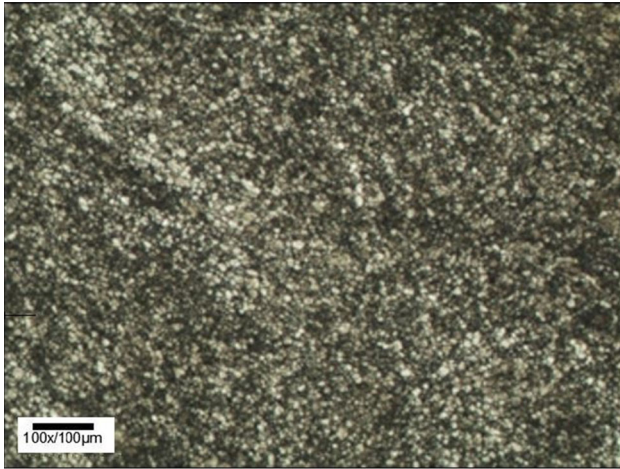


**Fig. 11** Microstructure of the weld nugget zone

**Fig. 12** Transmission electron microscope image (a) weld nugget zone showing very fine intragranular precipitates. (b) Heat-affected zone showing coarser precipitates

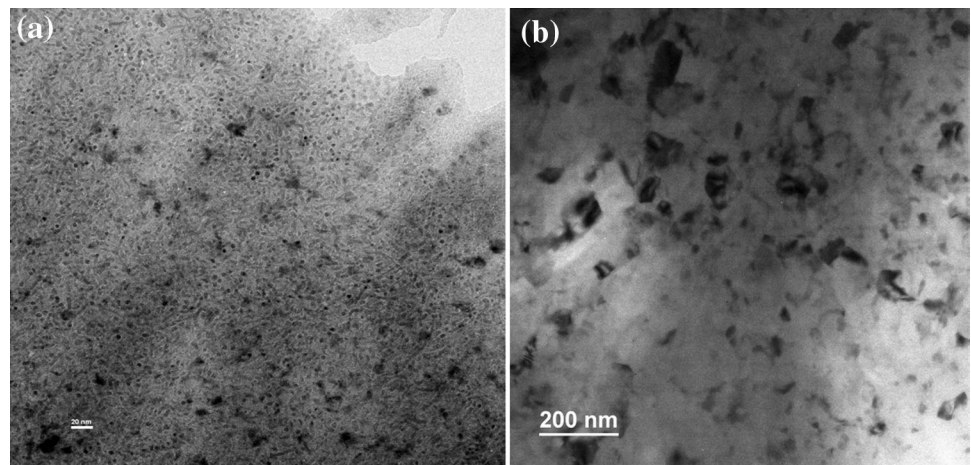
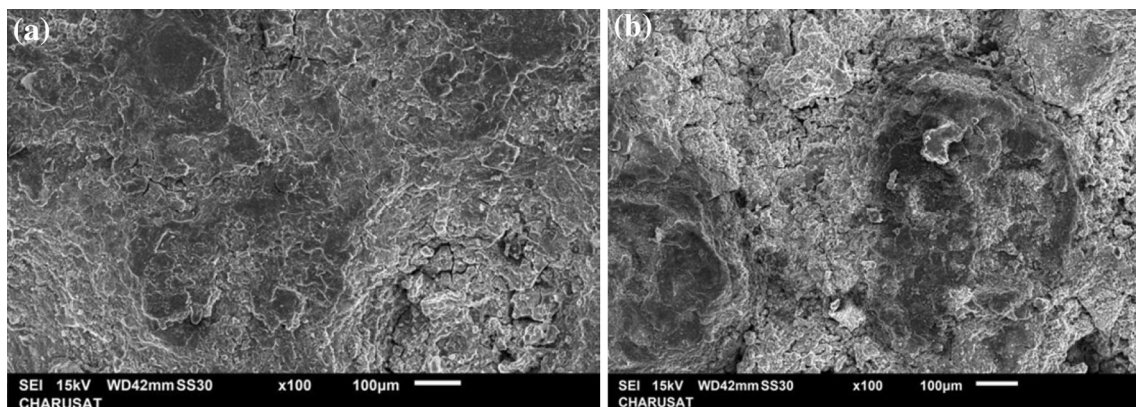


Fig. 10 taken at low magnification indicates that the HAZ is more vulnerable to corrosion as compared to the nugget zone. The major reason for this can be attributed to the variation in the grain size and the precipitate size of the WN and the HAZ. The heating and stirring action of the tool's pin results in smaller grains and fine intermetallics/precipitates in the nugget zone compared to the HAZ. The microstructure of nugget zone for plate C1 in Fig. 11 clearly shows the finer grain size. The optical micrograph does not reveal the presence of nanoscale precipitates in the nugget zone. However, TEM analysis of the nugget undertaken shows the presence of nanoscale precipitates in weld nugget. The TEM image of the nugget in Fig. 12a depicts the presence of very fine and dense intragranular precipitates in the WN zone. The TEM image of HAZ in Fig. 12b depicts the presence of coarser precipitates. It has been reported in previous findings for Al-Zn-Mg alloys that the composition of the precipitates in the weld nugget includes Mg and Zn [13, 28]. The anodic reaction during corrosion is controlled by the reduction in the grain size. The alloys that exhibit passivity in corroding environment shows an increase in corrosion resistance with



**Fig. 13** SEM image of corroded plate surface. (a) C1 and (b) C2

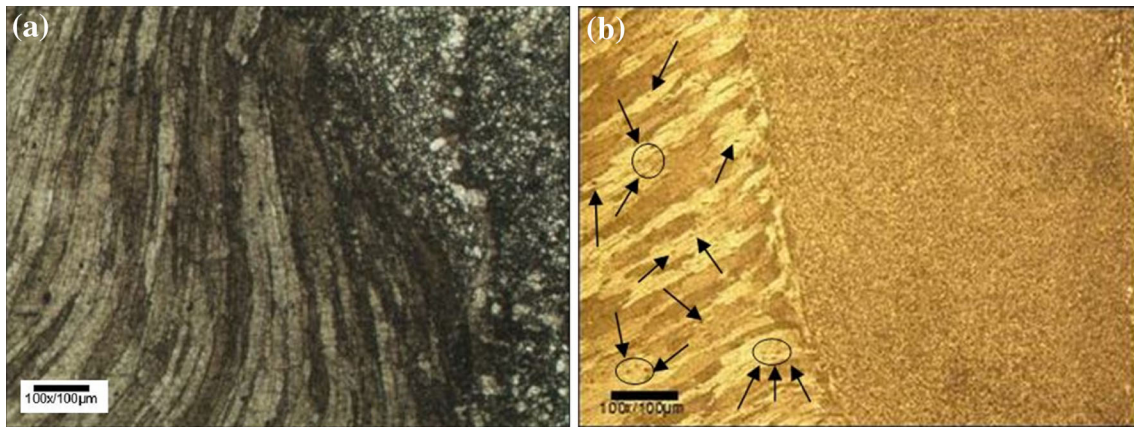


Fig. 14 Microstructure of nugget–TMAZ–HAZ interface. (a) C1 and (b) C2

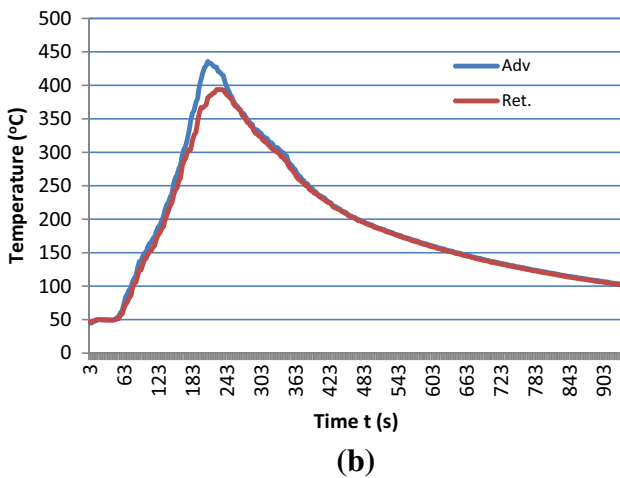
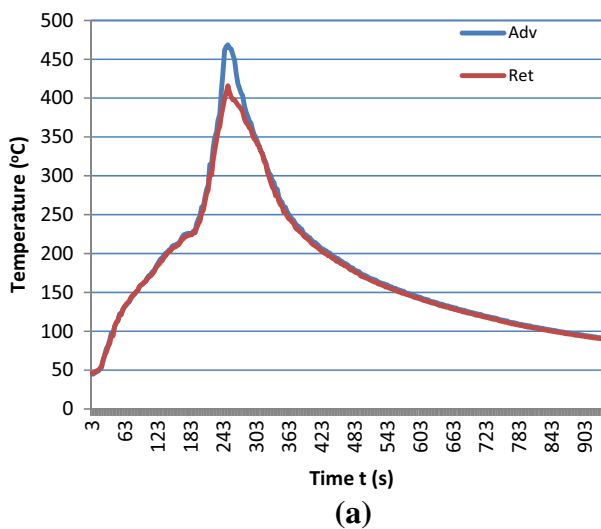


Fig. 15 Temperature profiles on advancing and retreating side. (a) C1 and (b) C2

grain refinement while the corrosion resistance decreases for other alloys [29]. Aluminum indicates passive behavior and the nugget which possesses relatively finer grain size

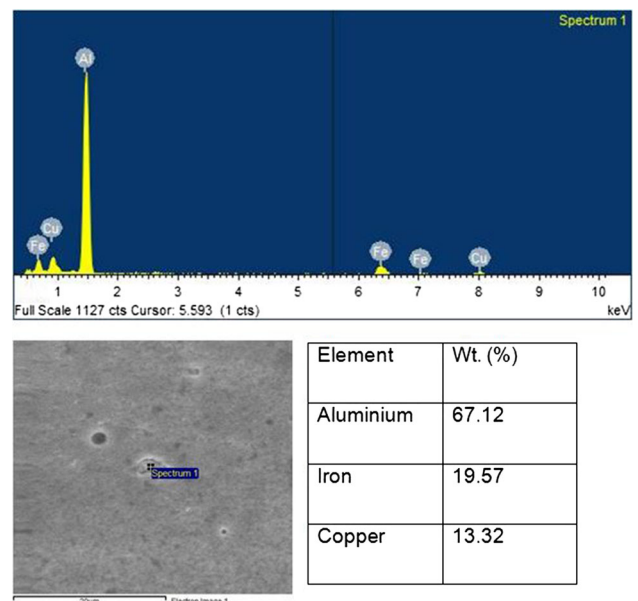
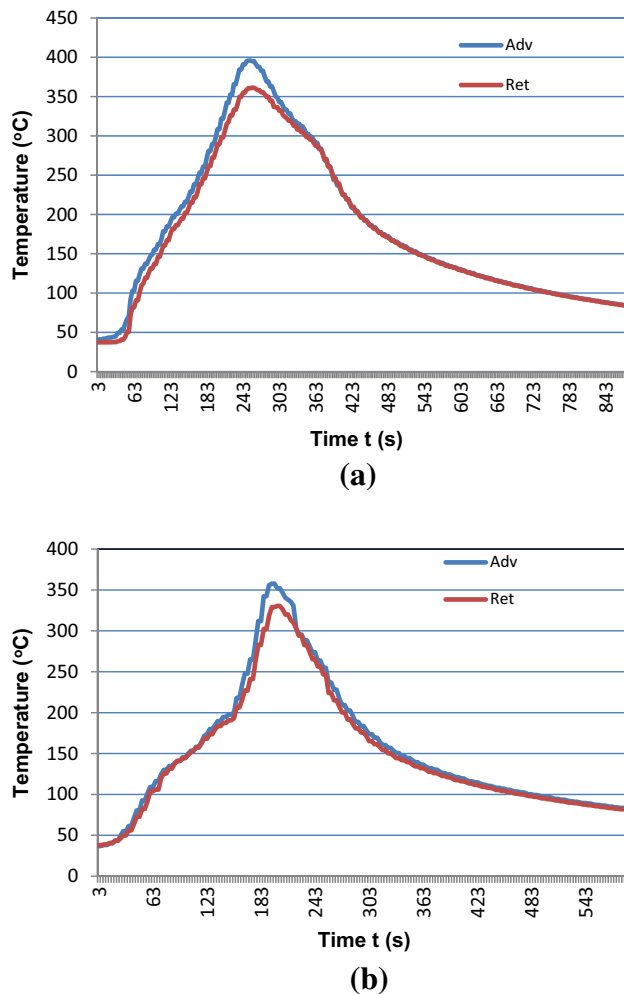


Fig. 16 SEM/EDX analysis of intermetallic in the hottest part of HAZ indicating Cu and Fe composition

and smaller size of precipitates compared to the HAZ will exhibit higher corrosion resistance. This clearly explains the lower corrosion susceptibility of the weld nugget compared to the HAZ (Ref. Figs. 7, 8, 9).

Further, SEM images of HAZ for the welded plates with different welding parameters have been investigated. The images of the nugget, TMAZ–HAZ and HAZ regions are studied under an optical microscope. The images taken with the help of optical microscope reveals that the response of the microstructure to welding is severe and the friction-stir-welded plates exhibit corrosion susceptibility where sensitization of the microstructure occurs.





**Fig. 17** Temperature profiles on advancing and retreating side. (a) C3 and (b) C4

### Effect of Tool Rotation Speed

Figure 13 shows the SEM images of HAZ of the corroded plates welded with 1500 rpm (C1) and 765 rpm (C2) tool rotation speeds, respectively. The SEM images clearly indicate that the surface degradation for plates C2 is much severe than the plates C1 indicating that the plates welded with lower tool rotation speed are more susceptible to corrosion. The images clearly reveal intergranular corrosion located along the heat-affected region. The optical micrographs of the nugget–TMAZ–HAZ interface for samples C1 and C2 are shown in Fig. 14. It is observed from the optical micrograph in Fig. 14b that there exist densely populated intermetallic/precipitates in plate C2 in the hottest region of HAZ. Figure 14a shows the same area for plate C1 which depicts that the intermetallic/precipitates are scarcely distributed. The major reason for such a kind of intermetallic/precipitates distribution is the difference in the heat input during welding for both the samples. The thermal histories recorded on the advancing and the retreating sides for both the welding conditions (C1 and C2) are shown in Fig. 15. The positions of the thermocouples to measure temperatures are so decided that they measure the temperatures just near to the rim of the tool shoulders, i.e., the TMAZ/HAZ interface zone. The average of the peak temperature recorded on the advancing and the retreating sides are reported here. The maximum temperatures recorded in the TMAZ/HAZ interface zone for plates C1 and C2 are 442.15 and 414.75 °C, respectively.

Keeping in view the importance of intermetallics in the corrosion behavior of the welded alloys, SEM/EDX is used to analyze the composition of the intermetallics. The intermetallics in the TMAZ/HAZ area were randomly

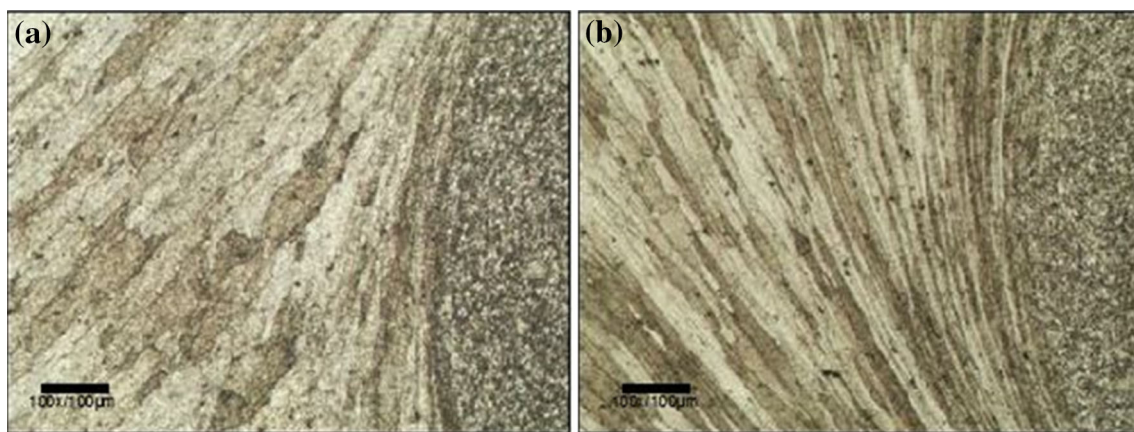


**Fig. 18** Microstructure of nugget–TMAZ–HAZ interface. (a) C3 and (b) C4

analyzed. The SEM/EDX analysis revealed that the intermetallics consisted of Al, Fe, and Cu in various proportions. Figure 16 shows the result of SEM/EDX analysis of one of the intermetallic. It is a well-established fact that intermetallics containing Fe and Cu are cathodic to the aluminum matrix. Thus, in the presence of a highly corroding medium, a high-pH environment is established at the noble particles. This results in the formation of grooves on the aluminum matrix around the intermetallics [30]. The parameters with higher heat input conditions result in higher dissolution of intermetallics/precipitates in the matrix. The lesser number of intermetallics results in a reduction in sites available for the cathodic activity in that location leading to a reduction in corrosion in these regions. Investigation on AA 2024-T3 undertaken by Bousquet et al. validates the fact that the severity of corrosion depends on the density and size of intermetallics at that location. Thus it can be concluded that the plates welded under relatively hotter welding conditions exhibit better corrosion resistance.

### Effect of Welding Speed

The plates welded with weld traverse speed of 20 mm/min (C3) and 50 mm/min (C4) subjected to EXCO immersion test for 48 h were analyzed with the help of optical microscope and SEM. During the welding process, the maximum temperatures recorded in the TMAZ/HAZ interface zone for plates C3 and C4 are 378.5 and 344.05 °C, respectively. It can be currently accepted that the maximum temperature during FSW raises with increasing tool rotational speeds and decreasing traverse speeds [2]. Figure 17 shows the temperature profiles recorded for C3 and C4 plates on the advancing and the retreating sides. The C3 plates have been welded with a lower traverse speed than C4 and thus subjected to hotter welding conditions then compared to C4. Hence, the C3

plates will have lesser intermetallics/precipitates in the TMAZ/HAZ region compared to C4 plates. Figure 18 shows the TMAZ/HAZ regions of plates C3 and C4 confirms the same. The SEM images of the corroded plate surfaces of C3 and C4 are shown in Fig. 19. The SEM image in Fig. 19 and photographs in Fig. 8 indicate lower

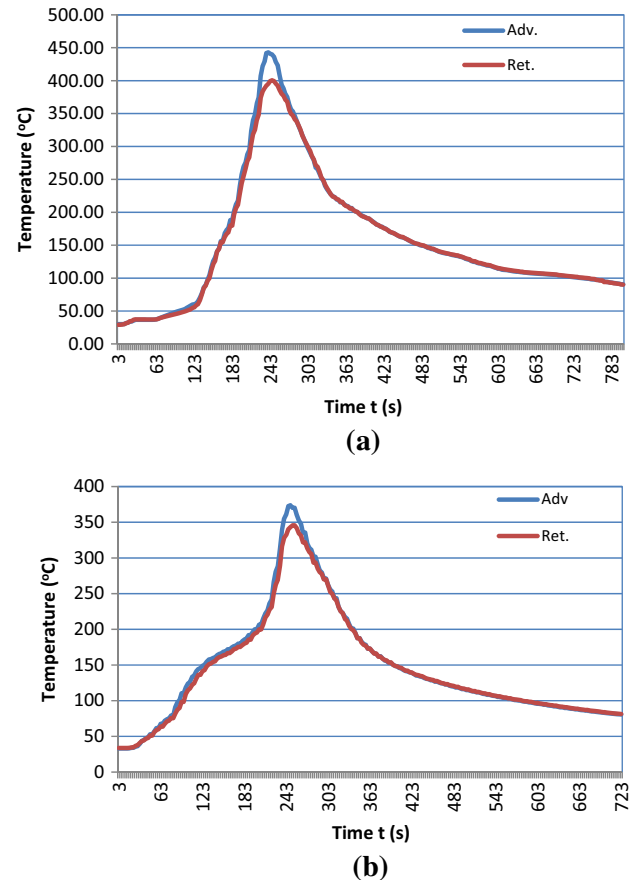


Fig. 20 Temperature profiles on advancing and retreating side. (a) C5 and (b) C6

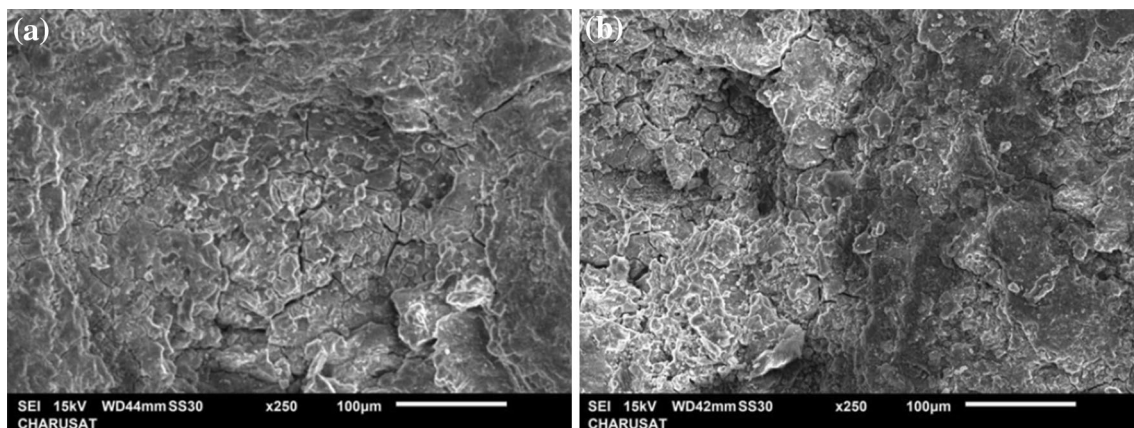


Fig. 19 SEM images of corroded plate surface. (a) C3 and (b) C4



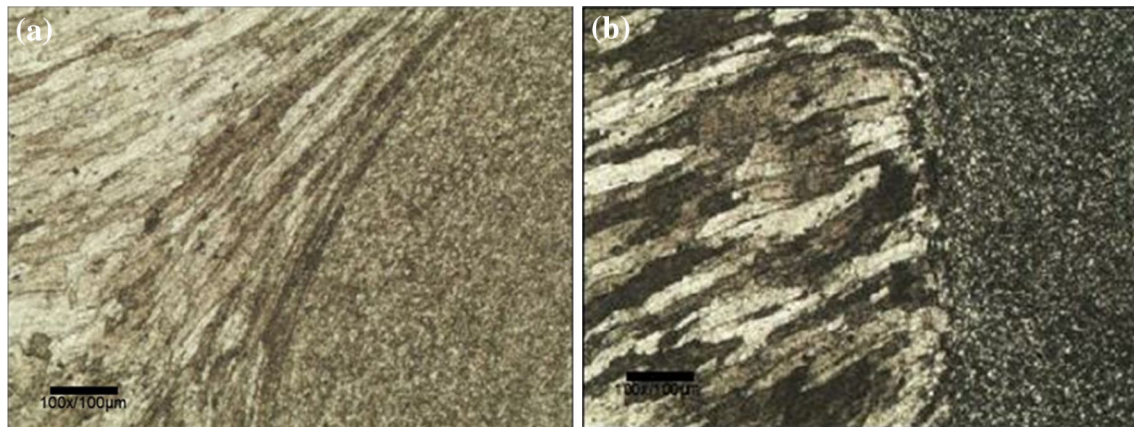


Fig. 21 Microstructure of nugget–TMAZ–HAZ interface. (a) C5 and (b) C6

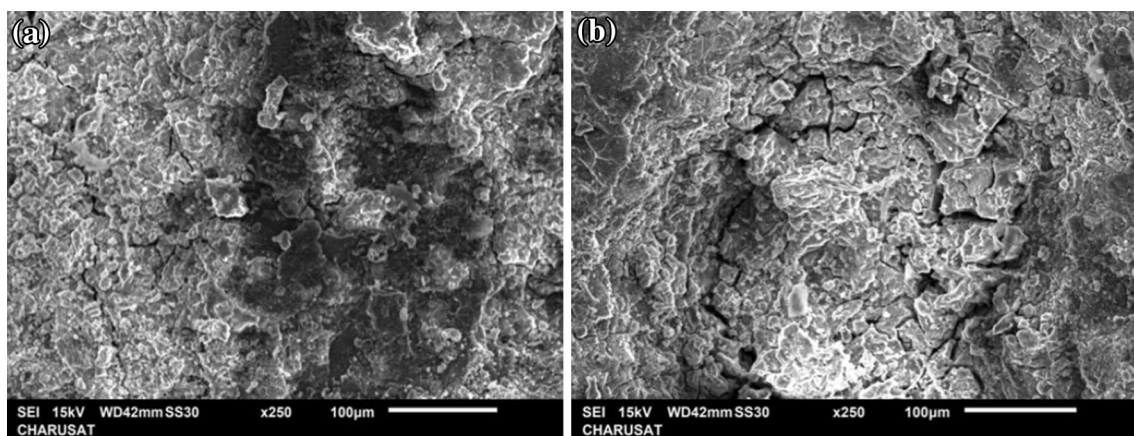


Fig. 22 SEM images of corroded plate surface. (a) C5 and (b) C6

pitting/exfoliation on plates welded at lower weld traverse speed (C3) compared to the plates welded at higher traverse speed (C4). The welding parameters for C3 produce a hotter weld compared to the parameters for C4. It again establishes the fact that the hotter friction stir welds are less susceptible to weld corrosion.

### Effect of Shoulder Diameter

The plates welded with shoulder diameter of 22 mm (C5) and 18 mm (C6) subjected to EXCO immersion test for 48 h were analyzed with the help of optical microscope and SEM. During the welding process, the maximum temperatures recorded in the TMAZ/HAZ interface zone for plates C5 and C6 are 421.65 and 359.70 °C, respectively. Figure 20 shows the temperature profiles recorded for C5 and C6 plates on the advancing and the retreating sides. The C5 plates have been welded with higher shoulder diameter than C6 and thus subjected to hotter welding conditions then compared to C6. Hence, the plates C5 will have lesser intermetallics/precipitates in the TMAZ/HAZ

region compared to C6 plates. Figure 21 showing the TMAZ/HAZ regions of plates C5 and C6 confirms the same. The SEM images of the corroded plate surfaces of C5 and C6 are shown in Fig. 22. The SEM image in Fig. 22 and photographs in Fig. 9 indicate lower pitting/exfoliation on plates welded at higher shoulder diameter (C5) compared to the plates welded at lower shoulder diameter (C6). The welding parameters for C5 produce a hotter weld compared to the parameters for C6. The hotter friction stir weld has higher corrosion resistance.

Thus, from the above investigation, it can be concluded that the lower corrosion susceptibility of the plates welded at hotter welding conditions can be attributed to the fact that, at higher temperatures, there will be a reduction in the number and size of the second-phase precipitates in the weld nugget. The number and size of the intermetallics in the HAZ of the weld is also influenced by the temperature during welding. At higher temperatures, the intermetallics dissolve in the matrix resulting in a reduction in the number and coarsening of the intermetallics. FSW of the alloys undertaken with parameters generating higher heat input



(i.e., higher tool rotation speed, lower weld travel speed and higher shoulder diameter) would produce a weld with lesser number of intermetallics/precipitates in the HAZ and thereby resulting into higher resistance to weld corrosion.

## Conclusions

- The pitting corrosion susceptibility of the HAZ is more than that the nugget and the base metal. The corrosion resistance is found in the order—weld nugget > unwelded base metal > HAZ.
- The hottest region of the HAZ was found to be the most corrosion susceptible part.
- The elevated temperatures associated with the FSW process results in sensitization of the microstructure which influences the corrosion resistance of the welded alloy.
- Corrosion resistance increases with the increase in the tool rotation speed from 765 to 1500 rpm with other parameters kept constant.
- Corrosion resistance decreases with the increase in the weld traverse speed from 20 to 50 mm/min with other parameters kept constant.
- Corrosion resistance increases with the increase in the shoulder diameter from 18 to 22 mm with other parameters kept constant.
- This clearly reveals that FSW joints are more corrosion resistant when hotter welding conditions are employed during the process.
- The amount of dissolution/coarsening of intermetallics increases for hotter welds. This decreases the number of sites available for galvanic coupling. Thus the corrosion resistance of the hotter welds increases.

**Acknowledgements** The writers would sincerely like to thank Indian Space Research Organisation (ISRO), India, for the monetary assistance given through a R&D Project No. E33011/60/2010-V. Authors would like to thank Pandit Deendayal Petroleum University (PDPU), Gandhinagar, India, for their help in providing a platform for conducting the experimental work required for the investigation.

## References

1. S. Rajakumar, C. Muralidharan, V. Balasubramanian, Influence of friction stir welding process and tool parameters on strength properties of AA7075-T6 aluminium alloy joints. *Mater. Des.* **32**(2), 535–549 (2011)
2. D.M. Rodrigues, A. Loureiro, C. Leitao, R.M. Leal, B.M. Chaparro, P. Vilaça, Influence of friction stir welding parameters on the microstructural and mechanical properties of AA 6016-T4 thin welds. *Mater. Des.* **30**(6), 1913–1921 (2009)
3. A.H. Feng, D.L. Chen, Z.Y. Ma, Microstructure and cyclic deformation behavior of a friction-stir-welded 7075 Al alloy. *Metall. Mater. Trans. A* **41**(4), 957–971 (2010)
4. B.T. Gibson, D.H. Lammlein, T.J. Prater, W.R. Longhurst, C.D. Cox, M.C. Ballun, K.J. Dharmaraj, G.E. Cook, A.M. Strauss, Friction stir welding: Process, automation, and control. *J. Manuf. Process.* **16**(1), 56–73 (2014)
5. R.K. Gupta, P. Ramkumar, B.R. Ghosh, Investigation of internal cracks in aluminium alloy AA7075 forging. *Eng. Fail. Anal.* **13**(1), 1–8 (2006)
6. H.K. Rafi, G.D.J. Ram, G. Phanikumar, K.P. Rao, Microstructure and tensile properties of friction welded aluminum alloy AA7075-T6. *Mater. Des.* **31**(5), 2375–2380 (2010)
7. M.W. Mahoney, C.G. Rhodes, J.G. Flintoff, W.H. Bingel, R.A. Spurling, Properties of friction-stir-welded 7075 T651 aluminum. *Metall. Mater. Trans. A* **29**(7), 1955–1964 (1998)
8. M. Selvaraj, M. Vela, S.R. Koteswara Rao, Mechanism of weld formation during friction stir welding of aluminum alloy. *Mater. Manuf. Process.* **28**(5), 595–600 (2013)
9. K. Deepandurai, R. Parameshwaran, Multiresponse optimization of FSW parameters for cast AA7075/SiCp composite. *Mater. Manuf. Processes* **31**(10), 1333–1341 (2016)
10. K.V. Jata, S.L. Semiatin, Continuous dynamic recrystallization during friction stir welding of high strength aluminum alloys. *Scr. Mater.* **43**(8), 743–749 (2000)
11. C.G. Rhodes, M.W. Mahoney, W.H. Bingel, R.A. Spurling, C.C. Bampton, Effects of friction stir welding on microstructure of 7075 aluminum. *Scr. Mater.* **36**(1), 69–75 (1997)
12. P.L. Threadgill, A.J. Leonard, H.R. Shercliff, P.J. Withers, Friction stir welding of aluminium alloys. *Int. Mater. Rev.* **54**(2), 49–93 (2009)
13. A.O. Mosleh, F.H. Mahmoud, T.S. Mahmoud, T.A. Khalifa, Microstructure and static immersion corrosion behavior of AA7020-O Al plates joined by friction stir welding. *Proc. Inst. Mech. Eng. L J. Mater. Des. Appl.* **230**(6), 1030–1040 (2015)
14. A. Behnagh, G. Besharati, M. Akbari, Mechanical properties, corrosion resistance, and microstructural changes during friction stir processing of 5083 aluminum rolled plates. *Mater. Manuf. Process.* **27**(6), 636–640 (2012)
15. D.A. Dragatogiannis, E.P. Koumoulos, I. Kartsonakis, D.I. Pantelis, P.N. Karakizis, C.A. Charitidis, Dissimilar friction stir welding between 5083 and 6082 Al alloys reinforced with TiC nanoparticles. *Mater. Manuf. Process.* **31**(16), 2101–2114 (2016)
16. J.B. Lumsden, M.W. Mahoney, G. Pollock, C.G. Rhodes, Intergranular corrosion following friction stir welding of aluminum alloy 7075-T651. *Corrosion* **55**(12), 1127–1135 (1999)
17. F.M. Khoshnaw, R.H. Gardi, Effect of aging time and temperature on exfoliation corrosion of aluminum alloys 2024-T3 and 7075-T6. *Mater. Corros.* **58**(5), 345–347 (2007)
18. T. Venugopal, K. Srinivasa Rao, K. Prasad Rao, Studies on friction stir welded AA 7075 aluminium alloy. *Trans. Indian Inst. Met.* **57**(6), 659–663 (2004)
19. F. Andreatta, H. Terryn, J.H.W. de Wit, Corrosion behaviour of different tempers of AA7075 aluminium alloy. *Electrochim. Acta* **49**(17–18), 2851–2862 (2004)
20. C.S. Paglia, M.C. Carroll, B.C. Pitts, T. Reynolds, R.G. Buchheit, Strength, corrosion, and environmentally assisted cracking of a 7075-T6 friction stir weld. *Mater. Sci. Forum* **396–402**, 1677–1684 (2002)
21. J. Kang, R.-D. Fu, G.-H. Luan, C.-L. Dong, M. He, In-situ investigation on the pitting corrosion behavior of friction stir welded joint of AA2024-T3 aluminium alloy. *Corros. Sci.* **52**(2), 620–626 (2010)
22. Rajesh, S., Badheka, V.J.: Effect of friction stir lap weld and post weld heat treatment on corrosion behavior of dissimilar aluminum alloys, in *Proceedings of the Institution of Mechanical Engineers, Part L: Journal of Materials: Design and Applications*. 1464420717692150 (2017)

23. G. Elatharasan, V.S. Senthil Kumar, Corrosion analysis of friction stir-welded AA 7075 Aluminium Alloy. *J. Mech. Eng.* **60**(1), 29–34 (2014)
24. I.J. Polmear, *Light Alloys—Metallurgy of the light metals*, 3rd edn. (Arnold Publishers, London, 1995)
25. C.S. Paglia, R.G. Buchheit, A look in the corrosion of aluminum alloy friction stir welds. *Scr. Mater.* **58**(5), 383–387 (2008)
26. W. Tian, S. Li, B. Wang, J. Liu, M. Yu, Pitting corrosion of naturally aged AA 7075 aluminum alloys with bimodal grain size. *Corros. Sci.* **113**, 1–16 (2016)
27. A. Chemin, D. Marques, L. Bisanha, A.D.J. Motheo, W.W. Bose Filho, C.O.F. Ruchert, Influence of Al7Cu2Fe intermetallic particles on the localized corrosion of high strength aluminum alloys. *Mater. Des.* **53**, 118–123 (2014)
28. S. Rajesh, V. Badheka, Influence of heat input/multiple passes and post weld heat treatment on strength/electrochemical characteristics of friction stir weld joint. *Mater. Manuf. Process.* **33**(2), 156–164 (2018)
29. K.D. Ralston, N. Birbilis, C.H.J. Davies, Revealing the relationship between grain size and corrosion rate of metals. *Scr. Mater.* **63**(12), 1201–1204 (2010)
30. K. Srinivasa Rao, K. Prasad Rao, Pitting corrosion of heat-treatable aluminium alloys and welds: a review. *Trans. Indian Inst. Met.* **57**(6), 593–610 (2004)